Atmospheric Research 236 (2020) 104816

Contents lists available at ScienceDirect

Atmospheric Research

journal homepage: www.elsevier.com/locate/atmosres

Study on CCN activity of fission product aerosols (CsI and CsOH) and their effect on size and other properties

Gaurav Mishra[a], S.N. Tripathi[b,c,*], T. Saud[d], Manish Joshi[e], Arshad Khan[e], B.K. Sapra[e]

[a] Nuclear Engineering and Technology Programme, Department of Mechanical Engineering, IIT Kanpur 208016, India
[b] Department of Civil Engineering, IIT Kanpur 208016, India
[c] Centre for Environmental Science and Engineering, IIT Kanpur 208016, India
[d] National Aerosol Facility, IIT Kanpur 208016, India
[e] Radiological Physics and Advisory Division, Bhabha Atomic Research Centre, Mumbai 400085, India

ARTICLE INFO

Keywords:
CCN
Cloud Condensation Nuclei
CsI
CsOH
Fission product aerosols

ABSTRACT

This paper discusses the size resolved cloud condensation nuclei (CCN) properties of two cesium bound compounds viz. CsI and CsOH. These properties are important in context of risk analysis and management of probable environmental releases during postulated nuclear reactor accident conditions. If released as fission product aerosols, these particles have potential to act as CCN, when exposed to humid environment. On activation, their evolution-deposition dynamics and consequently fate is expected to be affected in closed and/or open atmosphere. Size resolved CCN efficiency spectra (20–300 nm) are obtained for 0.2–1% supersaturation (SS) for pure CsI and CsOH particles employing a DMT-CCN counter. The essential parameters estimated from these measurements are activation diameter and size-averaged hygroscopicity (κ) at targeted SS levels. Experimental results were also compared with the standard theories available in the literature. Accuracy of the deposition rates for these particles (if released) in reactor component systems estimated by nuclear reactor accident analyses codes will improve when CCN properties are also taken into account. CCN efficiency spectra and activation diameters at specific SS for CsI and CsOH particles are being reported for the first time. Information on these properties strengthen the database which is vital for simulating behavioral characteristics of these particles. This in turn has capability to improve environmental source term estimations in the most unlikely scenario of containment breach during severe reactor accident conditions.

1. Introduction

In the event of a postulated nuclear reactor accident, the core of the reactor melts and fission products are released rapidly through the reactor coolant system to the containment building. In the containment, the aerosols of fission products may grow in the humid atmosphere and eventually settle onto the floor and water pools (Jokiniemi, 1988). In such an accident, the worst scenario is containment failure, where the integrity of the reactor building is lost soon after the accident before the fission products have had time to settle. An estimate reveals that as much as 80% of the fission products released from the reactor core may get deposited to the surfaces of the primary coolant circuit (Wright, 1994). Due to the decay heat of the reactor fuel, the deposited fission products may release at a later stage of an accident and emerge from the reactor coolant system days or even weeks after the accident (Wright, 1994). In case of a late containment failure it could lead to a major release of volatile fission products like cesium, iodine and tellurium to the environment.

Radioactive cesium, contributes to both external and internal radiation doses, has a half-life of 30 years and has contaminated > 2,00,000 km^2 of Europe after Chernobyl Disaster (Ramana, 2006). Studies have shown that around 6% of the European territory has been contaminated for more than $20 kilo - becquerel/m^2$ after the Chernobyl accident. The total amount of deposited cesium-137 in Europe is $8 * 10^{16}$ becquerel and the major part of this amount affects European countries in the following manner: Belarus 33.5%, Russia 24%, Ukraine 20%, Sweden 4.4%, Finland 4.3%, Bulgaria 2.8%, Austria 2.7%, Norway 2.3%, Romania 2.0%, Germany 1.1% (Izrael et al., 1996). Vast studies have been done in order to understand the effect of cesium in food chain, air, water and soil contamination as well as on livestock after Chernobyl Disaster (Paasikallio et al., 1994; Thomas and Martin, 1986; Mattsson and Moberg, 1991; Davidson et al., 1987; Lavi et al., 2006; Vakulovsky et al., 1994; Koulikov and Ryabov, 1992).

Radionuclides of cesium were identified in large amounts at

* Corresponding author at: Department of Civil Engineering, IIT Kanpur 208016, India.
E-mail address: snt@iitk.ac.in (S.N. Tripathi).

https://doi.org/10.1016/j.atmosres.2019.104816
Received 8 July 2019; Received in revised form 7 November 2019; Accepted 19 December 2019
Available online 24 December 2019
0169-8095/

numerous places, months after the Fukushima Daiichi Nuclear Power Plant disaster (Long et al., 2012). Estimate of release amounts of cesium and its compounds released into the atmosphere after nuclear reactor accidents have been discussed in detail in various studies (Jokiniemi, 1990; Yoschenko et al., 2006; Stohl et al., 2012). A study conducted by Stohl et al., 2012 reveals a cesium activity release of 9 to 36 petabecquerel(PBq) after the Fukushima Daiichi Nuclear Power Plant disaster (Stohl et al., 2012). Fission product vapors such as CsI and tellurium get released and condense on the particles in cooler regions above the core (Petti, 1989). In the presence of steam, CsI may convert to CsOH and a combination of CsI and CsOH is expected to be retained in containment following severe accident conditions (Mishra et al., 2019). CsI and CsOH are hygroscopic on account of high water solubility and get dissolved in water until the equilibrium vapor pressure of the solution is equal to the partial pressure of water vapor in the ambient atmosphere (Allelein et al., 2009). This water adsorption/absorption causes the particles to grow and the nature of growth can be quite dramatic in the case of pure CsI or CsOH particles. Particle growth to the equilibrium size can occur very rapidly i.e. in seconds. Because of the hygroscopic growth, settling velocities of these particles are higher in a humid environment than would be expected based on their dry sizes and even growth by coagulation or condensation (Allelein et al., 2009; Dwivedi et al., 2019).

Chemical composition and physical properties are major responsible parameters for aerosol particles to become cloud droplets and only a fraction of all particles are capable to grow into cloud droplets. The particles that can grow into cloud droplets (activate) under atmospheric supersaturations are cloud condensation nuclei (CCN). The supersaturation at which the particles get activated, is called critical supersaturation (S_c). CCN play an important role in the formation of clouds and precipitation, and they influence atmospheric chemistry and physics, the hydrological cycle, and climate (Rose et al., 2008). Many studies conclude that the abundance and properties of CCN may also affect precipitation amount and intensity, severe weather events and atmospheric dynamics (Andreae et al., 2004; Rosenfeld and Givati, 2006). The determination of the ability of particles to act as CCN under relevant atmospheric conditions is a crucial underlying challenge (McFiggans et al., 2006). The activation of CCN is determined by particle size and composition as well as water vapor supersaturation (Charlson et al., 2001; Segal et al., 2004; Andreae et al., 2005, Andreae et al., 2007; McFiggans et al., 2006). Reliable measurement data of CCN concentration and size distribution as a function of water vapor supersaturation are required for the quantitative description, understanding, and assessment of the effects of aerosols and its impact on the environment. Therefore, CCN measurements for different particles/contexts have been performed in laboratory and field experiments around the globe (Gunthe et al., 2009; Koehler et al., 2009; Hiranuma et al., 2011; Bhattu and Tripathi, 2014; Dalirian et al., 2015; Li et al., 2018; Duan et al., 2018; Tang et al., 2019; Ran et al., 2019; Hudson and Noble, 2014a,b; Hudson and Xie, 1999; Hudson and Yum, 2002; Yum and Hudson, 2001, 2004; Twohy et al., 2001). On the other hand, such studies don't exist for the particles that could be important for nuclear reactor accident research.

Fission product aerosols viz. CsI and CsOH, may get released to the atmosphere at the time of containment failure during severe nuclear reactor accidents and may act as CCN if exposed to sufficient relative humidity. Rain is responsible for wash-out (collection of particles by falling rain drops) and rain-out (formation of rain drops around the particles) of radionuclides from the atmosphere which results in a greater contamination of ground surfaces (Madoz-Escande et al., 2005). A detailed study has already been done to estimate the hygroscopic behaviour of these cesium particles in subsaturated environmental conditions (Mishra et al., 2019) in which it was found that CsI particles grow suddenly above 91% relative humidity while CsOH shows a continuous growth when exposed to increasing relative humidity. The behavior of these cesium compounds in supersaturated conditions is an link to the information available for subsaturated conditions. Various properties (e.g. condensational growth, deposition rate etc.) of cesium compounds have been studied (Acquista et al., 1968; Badawi et al., 2012; Inade and Akagane, 1996; Kuczkowski et al., 1966; Li et al., 2013; McFarlane et al., 2002) but the CCN properties have not been given due attention. Such information is important for estimating characteristics of CCN released due to a containment breach and as a source term to the environment in the event of a severe nuclear reactor accident (Camata et al., 2000). Moreover, CCN behaviour of CsI and CsOH is much needed to supplement the predictive capability of numerical models against source term estimates and risk-hazard evaluations.

In the present study, several experiments have been performed by exposing CsI and CsOH particles of known dry size to known supersaturation, and then varying the sizes and/or supersaturations to estimate the behaviour of these compounds to act as CCN. CCN efficiency spectra have been generated for pure CsI and CsOH compounds from the results of the measurements. Results have also been compared with the standard theories in the literature.

2. Experimental section and data analysis

2.1. Instrumentation and measurements

Initially the test solutes were dissolved in MilliQ water (typically 0.1 g/L, resistivity = 18:2 $M\omega cm$) and aerosolized through an aerosol atomizer (TOPAS ATM 226). 0.1 M salt solutions (CsI, purity > 99.5%, Merck; CsOH, purity > 99%, Merck) were used for pure salt experiments. A perspex chamber of $0.5m^3$ volume was used to homogenize the generated particles and to provide a steady state concentration for the set-up connected at the exit port. Subsequently (Fig. 1), aerosol particles, passed through silica-gel based diffusion dryer (RH < 15% at 298 K), were imparted charge equilibrium through an aerosol conditioner (TSI 3077), and were classified with a Differential Mobility Analyser (DMA) (TSI DMA 3081; Sample flow rate = 0.8 lpm and sheath flow rate = 8 lpm). On the basis of electrical mobility, particles were size-classified in the DMA. These monodispersed particles were measured and characterized by Droplet Measurement Technologies Continuous-Flow Streamwise Thermal-Gradient CCN counter (CCN-100; Flow rate = 0.5 lpm; Sheath to aerosol ratio = 10:1) and Condensation Particle Counter (CPC) (TSI CPC 3776; Flow rate = 0.3 lpm). The DMT CCN counter (CCN-100) has been widely used to determine the CCN concentration in various laboratory and atmospheric studies (Gunthe et al., 2009; Koehler et al., 2009; Hiranuma et al., 2011; Padró et al., 2012; Bhattu and Tripathi, 2015; Dalirian et al., 2015; Loftus and Cotton, 2014; Bhattu et al., 2016; Che et al., 2017; Li et al., 2018). The detailed schematic of experimental setup is shown in Fig. 1.

Before starting the experiments, calibration of the CCN counter was done using monodisperse ammonium sulphate (purity > 99%, Merck) particles for different ΔT ranging from 3 to 16 K in order to calculate effective supersaturation, SS_{eff} as discussed by Rose et al., 2008 (Rose et al., 2008). In the present study to obtain size-resolved CCN activation spectra at seven selected supersaturation levels (0.2%, 0.3%, 0.4%, 0.5%, 0.6%, 0.8%, 1.0%), 15 different particle diameters (20 nm 300 nm with a step difference of 20 nm) were selected. Each diameter was allowed to run for 3 min at one supersaturation. At the start and end of sampling, the aerosol size distribution was taken from a Scanning Mobility Particle Sizer (SMPS) (TSI SMPS 3082; Sheath to aerosol ratio = 10:1). One full set of seven different supersaturations was covered in 345 mins that include sufficient adjustment time (=5 min.) between two supersaturation levels. The first 60 s of every 3 min data set is discarded, and the data integration time was kept at 120 s that included all the data points during that period.

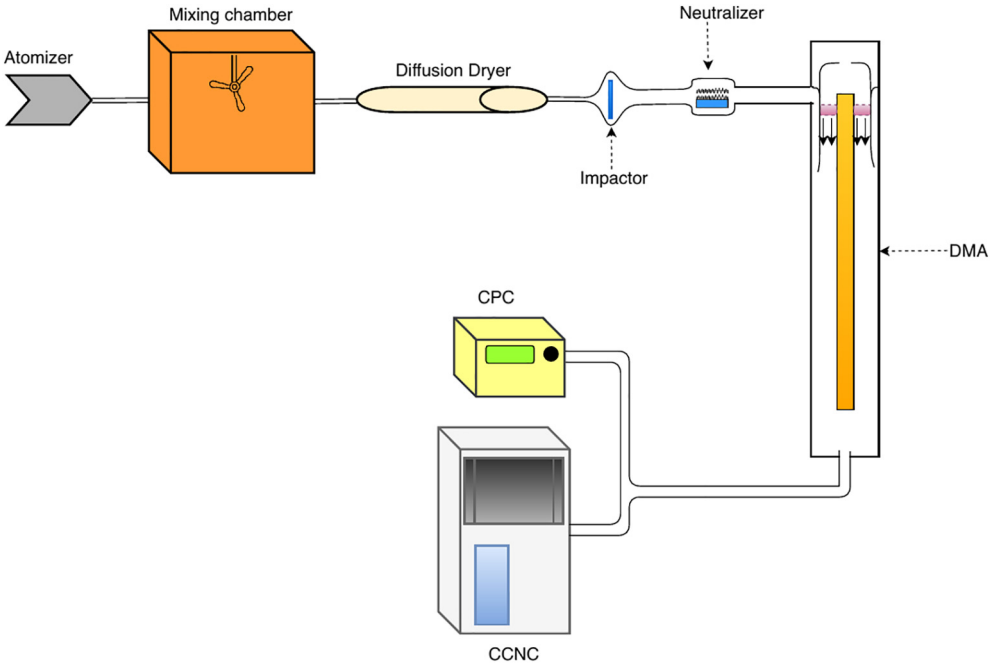

Fig. 1. Experimental setup.

2.2. Methodology

Multiply-charged particle corrections (Frank et al., 2006) and DMA transfer function correction (Rose et al., 2008) were applied to the entire size-resolved CCN efficiency spectra. For multiple charge correction, the aerosol size distribution measured by SMPS is used with an assumption that the size distribution did not vary significantly inside the chamber as steady state is maintained. The counting inefficiency correction for CCN and CPC was not needed in this study as for pure ammonium sulphate particles, the CCN/CN ratio reached unity for all ΔT considered. Also, the SS depletion correction was not applied because the total CCN concentration never reached the threshold value of 5000 $particlescm^{-3}$ during the experiments (Lathem and Nenes, 2011).

Each CCN efficiency spectrum was fitted with a cumulative Gaussian (normal) distribution function using a nonlinear least-squares fitting routine (Gauss-Newton method, Matlab, MathWorks, Inc.) as discussed by Rose et al., 2008 (Rose et al., 2008). Eq. (1) shows the fitting function in which

$$f_{\frac{CCN}{CN}} = a\left(1 + erf\left(\frac{D - D_a}{\sigma_a 2^{0.5}}\right)\right) \quad (1)$$

the fit parameters, a and σ_a are half of the maximum activated fraction (MAF = 2a), and standard deviation of the fit, respectively. D_a represents the dry particle diameter at which CCN/CN fraction reaches 50% of its maximum value. All these parameters correspond to properties of CCN active particles. MAF < 1 suggests the external mixing of CCN inactive particles with CCN active particles from D_a to D_{max}. σ_a shows the width of chemical distribution of CCN active particles. The heterogeneity parameter (σ_a/D_a) for single component system should be nearly zero in ideal conditions but for the ammonium sulphate (used for calibration in present study), it is found to be 3% which could be due to DMA transfer function effects, particle morphological effects, and changes in the supersaturation conditions of the system (Gunthe et al., 2009; Rose et al., 2010; Bhattu and Tripathi, 2014).

In the present study, the effect of chemical composition on CCN activity of aerosols is also parameterized by calculating the hygroscopicity parameter, κ, with the use of Eq. (2). κ accounts for not only the effect of solute on water activity, but also changes in surface tension and is based on Kohler theory (Petters and Kreidenweis, 2007; Rose et al., 2010).

$$S = \frac{D_{wet}^3 - D_a^3}{D_{wet}^3 - D_a^3(1-\kappa)} exp\frac{4\sigma_{sol}M_w}{RT\rho_w D_{wet}} \quad (2)$$

In Eq. (2), D_{wet} is diameter of the droplet at saturation ratio, $S = (1 + SS/100\%)$. κ is hygroscopicity parameter, which is calculated for $T = 298.15$ K, $\sigma_{sol} = 0.072J.\ m^{-2}$, $R = 8.315J.\ K^{-1}.\ mol^{-1}$, $\rho_w = 998.1kg.\ m^{-3}$ and $M_w = 0.018kg.\ mol^{-1}$. According to Gunthe et al., 2009, κ tells about the average hygroscopicity of CCN active particles in that particular size range around D_a (Gunthe et al., 2009). κ, for all pairs of supersaturation and activation diameter, was calculated according to the procedure discussed by Rose et al., (2010) (Rose et al., 2010). Eq. (1) is used for obtaining D_a from the Cumulative Gaussian Distribution function (CDF) fit of measured CCN/CN spectrum. Both D_{wet} and κ were varied until the difference between calculated saturation ratio (S in Eq. (2)) and the measured saturation ratio [$S_{measured} = 1 + (SS_{measured}/100\%)$] approached a minimum value.

With the help of Eq. (3), theoretical activation diameters for CsI and CsOH have been generated at each supersaturation as a part of this study.

$$D_a = \left[\frac{256M_w^3\sigma^3}{27R^3T^3\rho_w^3}\right]^{1/3}\left[\left(\frac{M_w}{\rho_w}\right)\left(\frac{\rho_s}{M_s}\right)\left(\frac{\varepsilon_s}{\nu_s}\right)\right]^{-1/3} S^{-2/3} \quad (3)$$

where S is supersaturation (%),M_w and ρ_w are molecular weight and density of water, and M_s and ρ_s are molecular weight and density of different solutes, ε_s is the volume fraction of solute, ν_s is the vant Hoff factor of solute, T is ambient temperature (Kelvin), σ is the droplet surface tension, the same as that of pure water and R is the gas constant (Padró et al., 2012; Bhattu and Tripathi, 2015).

3. Results and discussion

For quantitative evaluation of CCN activity, it is important to know particle size as well as the saturation-condition of the environment. As discussed earlier, CCN properties of CsI and CsOH particles have potential to modify the accuracy of source term to environment under reactor accident conditions. Measurements of CCN can help to understand the variation of their activation characteristics, and closure

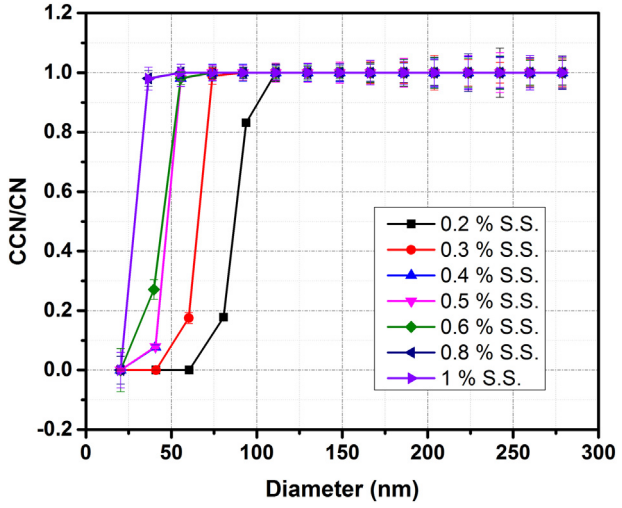

Fig. 2. Averaged size-resolved CCN efficiency spectra at different water vapor supersaturations (SS = 0.2%, 0.3%, 0.4% 0.5%, 0.6%, 0.8%, 1.0%) for CsI.

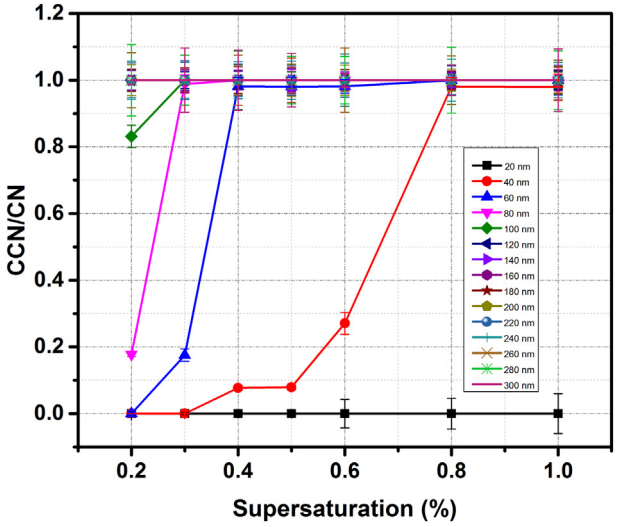

Fig. 3. Average CCN spectra as a function of supersaturation of CsI.

studies can be used to test our knowledge of the controlling physical and chemical factors, to determine the best prediction methods for CCN. In the present study the CCN activity is evaluated for CsI and CsOH using hygroscopicity parameter κ (Petters and Kreidenweis, 2007) which is estimated from the CCN activation diameter under controlled supersaturation (SS) conditions.

3.1. Cesium Iodide (CsI)

The average CCN efficiency spectra (*CCN/CN*) for pure Cesium Iodide (CsI) salt as a function of particle diameter and supersaturation is shown in Fig. 2 for different SS conditions. Each data point shown in Fig. 2 is the average value obtained from the CDF fit to the measured CCN efficiency spectra corresponding to the particular mobility diameter and the solid lines are showing Cumulative Gaussian Distribution fit. It has been observed that the particles with diameter > 100 nm are activated even at lower SS (SS = 0.2%). Critical supersaturation (S_c) is often associated with the supersaturation where 50% of the particles are CCN activatedequivalent to a *CCN/CN* ratio of 50%, and this convention is followed in this work although the two are not necessarily equal when the *CCN/CN* curve is not a step function. There is general agreement that the activation of CCN at a given level of supersaturation depends primarily on the particle size, followed by the chemical composition and the mixing status; however, the relative importance of these characteristics may vary greatly in different environments (Che et al., 2017). Fig. 3 alternatively displays activation ratio of 3 min averaged CCN efficiencies against supersaturation for pure CsI particles of different mobility diameters. As it is evident from Fig. 3, the critical supersaturation decreases with increasing particle diameter. At SS between 0.2 and 1%, the crucial size range for CCN activation is 20 to 100 nm. Particles much larger than D = 100 nm are generally activated at all investigated values of SS regardless of their composition, whereas particles < 20 nm require out-of-range high SS for activation. Between these two extremes, a strong dependence of CCN efficiency on particle size is apparent. Particles with diameters of 20 nm typically require SS of up to 0.8% for activation, whereas particles with diameters of 80 nm require SS of ~0.3%. Each CCN spectra (Fig. 2) is fitted using Eq. (1) to obtain activation diameter, D_a. The mean D_a of CsI were 87.05, 64.20, 46.65, 46.62, 43.32, 32.67 and 33.34 nm under the 0.2%, 0.3%,0.4%,0.5%, 0,6%, 0.8%, and 1% SS conditions respectively. The activation diameter increased with decreasing SS, and was found to be largest at SS = 0.2% (Fig. 2, Table 1). Experimentally and theoretically determined critical supersaturations of pure CsI particles as a function of particle activation diameter are shown in Fig. 4. It has been observed

Table 1
Average CDF fit parameters (D_a, MAF, σ_a, σ_a/D_a, κ) for CsI.

SS(%)	D_a	MAF	σ_a	σ_a/D_a	κ
0.2	87.05 ± 6.06	1	6.00 ± 0.08	0.069 ± 0.002	0.31 ± 0.15
0.3	64.20 ± 2.75	1	2.69 ± 0.07	0.042 ± 0.003	0.57 ± 0.10
0.4	46.65 ± 1.97	1	1.95 ± 0.03	0.042 ± 0.001	0.84 ± 0.14
0.5	46.62 ± 1.98	1	1.95 ± 0.04	0.042 ± 0.005	0.54 ± 0.09
0.6	43.32 ± 2.52	1	2.51 ± 0.03	0.058 ± 0.002	0.47 ± 0.11
0.8	32.67 ± 0.62	1	0.58 ± 0.05	0.018 ± 0.003	0.61 ± 0.05
1	31.34 ± 0.53	1	0.47 ± 0.06	0.015 ± 0.003	0.44 ± 0.02

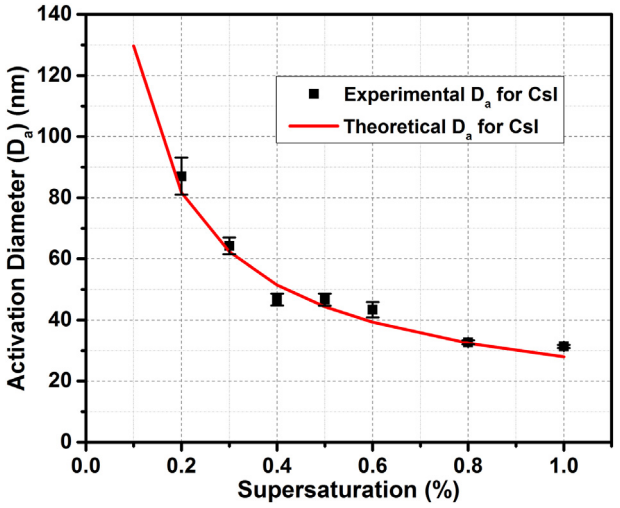

Fig. 4. Experimental and theoretical activation diameters for CsI.

that experimental and theoretical values of activation diameter as a function of supersaturation are well matched within the experimental domain. To estimate the critical supersaturations of pure soluble particles, κ-Kohler theory (Eq. (2)) has been applied. The value of κ represents the hygroscopicity of the particles and varies with chemical composition. Table 1 also lists κ values of the hygroscopic material CsI calculated in this study. The theoretical and experimental values of hygroscopicity parameter (κ) as a function of supersaturation are also presented in Fig. 5. As expected, CsI particles on account of their hygroscopic nature (see κ values in Table 1), activated at lower supersaturations like $(NH_4)_2SO_4$ at size 120 nm (Dalirian et al., 2015).

The average CCN number concentrations were calculated by

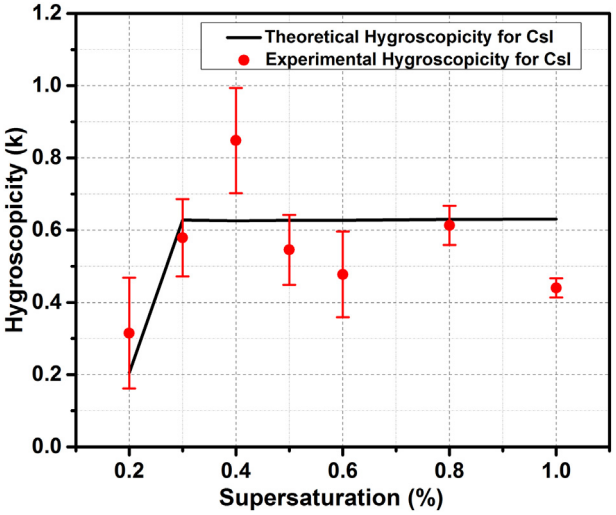

Fig. 5. Experimental and theoretical hygroscopicity for CsI.

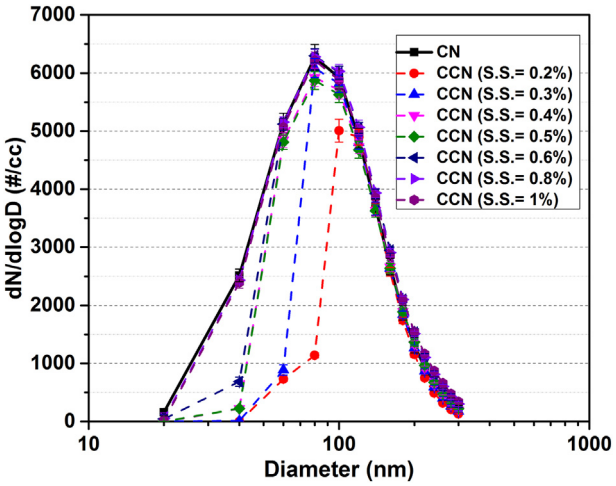

Fig. 6. Number size distribution of CN and CCN at SS = 0.2–1.0% for CsI.

multiplying the interpolated average CN size distribution by the average active fraction of the CCN. The average CCN and CN size distributions obtained during the measurement at seven different levels of supersaturation is shown in Fig. 6. Fig. 6 shows that the number size distributions of the CN and CCN were mono-modal. Almost all particles > 100 nm were activated at the measured supersaturations and no CCN were observed for particles of size 20 nm in this study.

By fitting with a cumulative Gaussian distribution function (CDF), the following parameters were derived from the three-parameter CDF of each measured CCN efficiency spectrum; the maximum activated fraction (*MAF*), the midpoint activation diameter D_a, and the standard deviation σ_a of CDF fits. The average activation parameters derived from the CDF are summarized in Table 1. Fig. 2 and Table 1 show that the maximum activation fraction (estimated from the fitting procedures as explained earlier) was unity at all levels of supersaturation. Therefore, at different values of SS, all particles of size > 100 nm are active CCN. Various past studies have shown the applicability of size-resolved CCN measurements in determining the probable mixing state of particles (Bhattu et al., 2016). Fig. 1 and Table 1 show that the critical active diameters for CCN-active particles (D_a, derived from the 3-parameter CDF fitting) varied from about 87 to 33 nm, with SS ranging from 0.2 to 0.8%. Hence, the average activation diameter (D_a) decreases with increase in SS. The ratios σ_a/D_a, i.e. the ratio of standard deviation and critical active diameter, which represent the degree of heterogeneity of CCN-active particles around D_a and the overall degree of heterogeneity of CCN-active particles, decreased with increasing diameter of the particles with an exception between 0.3 and 0.5% SS, showing that the larger particles were more homogeneous and more internally mixed.

The ability for ammonium sulfate particles to act as CCN has been widely studied (Garland, 1969; Kreidenweis et al., 2005; Hiranuma et al., 2011), and κ values of ammonium sulfate particles (Petters and Kreidenweis, 2007), are in good agreement with the κ value fitted to our results (0.37–0.84). The values of κ are almost consistent with the critical active diameters, indicating that hygroscopicity of CsI does not vary with particle diameters. The mean κ values of CsI observed were 0.5, 0.57, 0.84, 0.53, 0.46, 0.61 and 0.37 under the same SS conditions respectively. No specific trend of κ has been observed. The value of κ does not fall in the range of continental κ (0.27 ± 0.21) calculated by numerical model (Pringle et al., 2010). However, it is closer to the value of pure $(NH_4)_2SO_4$ (0.61; (Petters and Kreidenweis, 2007)).

3.2. Cesium Hydroxide (CsOH)

The average CCN efficiency spectra (CCN/CN) for pure Cesium hydroxide (CsOH) salt as a function of particle diameter and supersaturation is shown in Fig. 7 for different SS conditions. It is also seen that the particles with diameter > 100 nm are activated even at lower SS 0.2% like CsI. Fig. 8 shows CCN efficiencies and displays activation ratio against supersaturation for pure CsOH particles of different mobility diameters. Like CsI, here also the particles of 20 nm could not be activated even at higher values of SS (Fig. 8). Each CCN is fitted using Eq. (1) to obtain activation diameter, D_a. The mean D_a of CsOH were 86.42, 64.21, 48.18, 46.07, 46.03, 33.37 and 33.31 nm under the 0.2%, 0.3%,0.4%,0.5%, 0,6%, 0.8%, and 1% SS conditions respectively (Table 2). The activation diameter increased with decreasing SS, and was found to be largest at SS = 0.2% (Table 2). The critical supersaturation decreases with increasing particle diameter. Experimentally and theoretically determined critical supersaturations of pure CsOH particles as a function of particle mobility diameter are shown in Fig. 9 similar to CsI particles.

It is observed that the experimental and theoretical values of activation diameter as a function of supersaturation are well matched. The theoretical and experimental values of hygroscopicity as a function of supersaturation are also presented in Fig. 10. At SS between 0.2 and 1%, the crucial size range for CCN activation is 40 to 100 nm. Particles much larger than 100 nm are generally activated at all investigated values of SS, whereas particles < 40 nm require very high SS for activation. A strong dependence of CCN efficiency on particle size is

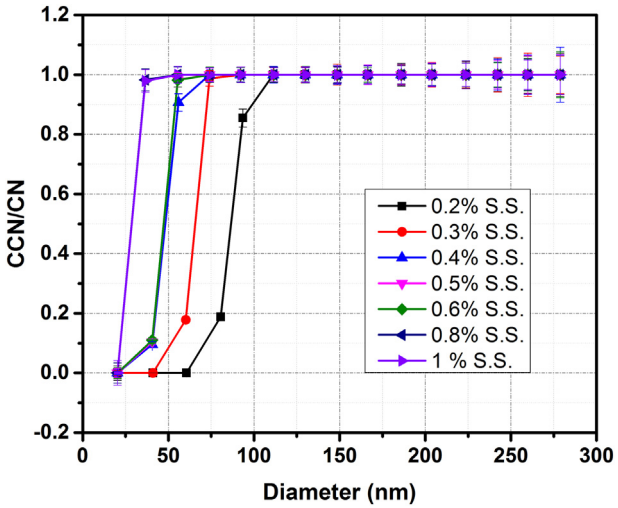

Fig. 7. Averaged size-resolved CCN efficiency spectra at different water vapor supersaturations (SS = 0.2%, 0.3%, 0.4% 0.5%, 0.6%, 0.8%, 1.0%) for CsOH.

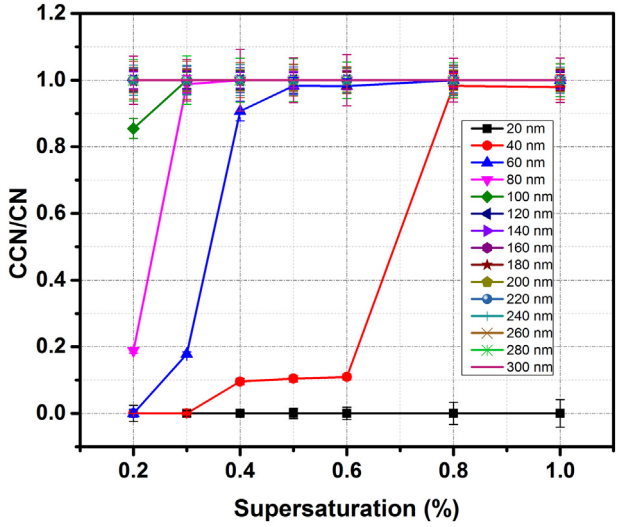

Fig. 8. Average CCN spectra as a function of supersaturation of CsOH.

Table 2
Average CDF fit parameters (D_a, MAF, σ_a, σ_a/D_a, κ) for CsOH.

SS(%)	D_a	MAF	σ_a	σ_a/D_a	κ
0.2	86.42 ± 5.76	1	5.70 ± 0.08	0.066 ± 0.004	0.32 ± 0.16
0.3	64.21 ± 2.79	1	2.76 ± 0.04	0.043 ± 0.005	0.57 ± 0.10
0.4	48.18 ± 2.81	1	2.79 ± 0.03	0.058 ± 0.003	0.77 ± 0.19
0.5	46.07 ± 2.03	1	2.02 ± 0.02	0.044 ± 0.002	0.56 ± 0.10
0.6	46.03 ± 2.07	1	2.07 ± 0.01	0.045 ± 0.001	0.39 ± 0.07
0.8	33.37 ± 0.50	1	0.50 ± 0.01	0.015 ± 0.002	0.57 ± 0.04
1	33.31 ± 0.53	1	0.53 ± 0.01	0.016 ± 0.002	0.36 ± 0.02

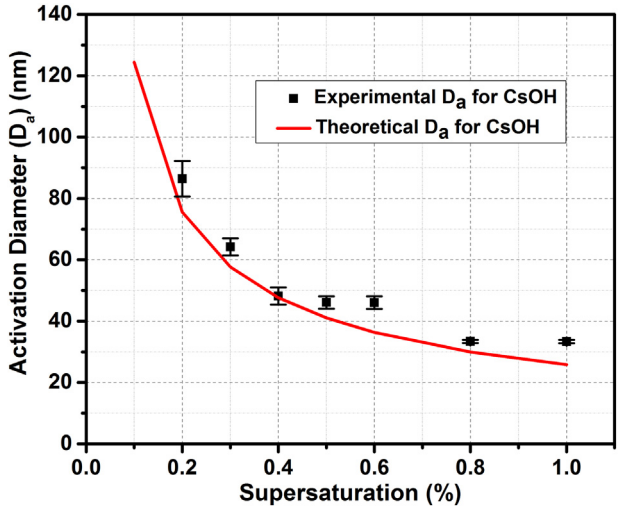

Fig. 9. Experimental and theoretical activation diameters for CsOH.

noticed. Particles with diameters of 40 nm typically require SS of up to 0.8% for activation, whereas particles with diameters of 60 nm require SS of ~0.5%. As expected, like CsI, CsOH particles are also highly hygroscopic particles (see κ values in Table 2), activated at lower supersaturations.

The average CCN and CN size distributions obtained during the measurement at seven different levels of supersaturation is shown in Fig. 11. The number size distributions of the CN and CCN were found to be mono-modal like CsI. Almost all particles > 200 nm were activated at the measured supersaturations and no CCN were observed for particles < 20 nm, showing the effect of particle size on the activation of CCN.

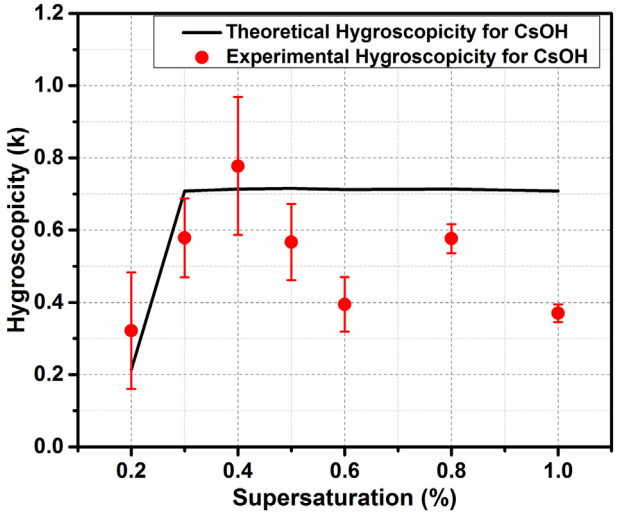

Fig. 10. Experimental and theoretical hygroscopicity for CsOH.

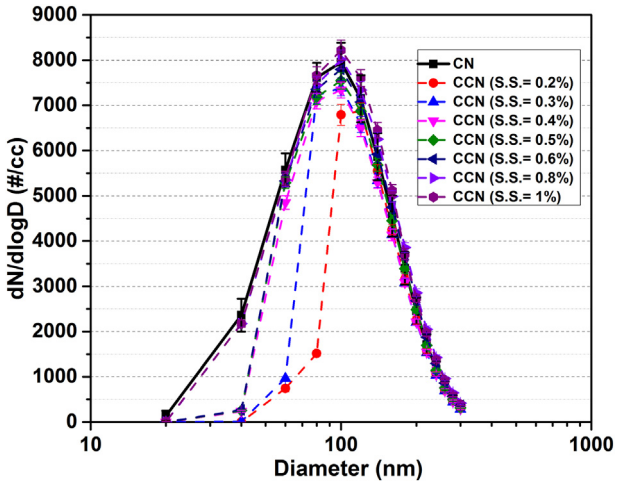

Fig. 11. Number size distribution of CN and CCN at SS = 0.2–1.0% for CsOH.

The average activation parameters derived from the CDF are summarized in Table 2. Fig. 7 and Table 2 show that the maximum active fraction (*MAF*, derived from the 3-parameter CDF fitting, detailed in Methods) was unity at all supersaturations. Therefore, at different values of SS, all particles irrespective of size are CCN. Fig. 8 and Table 2 show that the critical active diameters for CCN (D_a, derived from the 3-parameter CDF fitting) varied from about 87 to 33 nm, with SS ranging from 0.2 to 0.8%. Hence, like CsI, the average activation diameter (D_a) decreases with increase in SS. The overall degree of heterogeneity of CCN, decreased with increasing diameter of the particles, showing that the larger particles were more homogeneous and more internally mixed.

Table 2 lists κ values of the hygroscopic materials CsOH calculated in this study. The values of κ are almost consistent with the critical active diameters, indicating that hygroscopicity of CsOH does not vary with particle diameters. The mean κ values of CsOH observed were 0.52, 0.57, 0.77, 0.55, 0.39, 0.57 and 0.37 under the same SS conditions respectively. No specific trend of κ has been observed like CsI. Similar to CsI, the value of κ is closer to the value of pure $(NH_4)_2SO_4$ (0.61; (Petters and Kreidenweis, 2007)).

To derive the size distributions of CCN at a given SS, the size-resolved CCN spectra are combined with aerosol number size distributions. The CCN efficiencies are linearly interpolated to SS. The resulting dependence of CCN efficiency on particle size is then used to derive the

CCN size distributions (Figs. 6 and 11). For each value of SS, the CCN concentration gradually increases toward larger diameters (Figs. 6 and 11), instead of showing a sharp cutoff activation diameter, as expected from an internally mixed aerosol. This reflects a certain degree of external mixing in aerosols, as well as the fact that the particles are not exactly mono disperse (Frank et al., 2006).

4. Conclusions

Size-resolved CCN activity of aerosol particles is one of the key indices determining their evolution dynamics at high SS levels. This work focused on measuring and interpreting CCN properties of pure CsI and CsOH particles at various supersaturations. The parameters obtained from these results are CCN efficiency spectra, activation diameter and size-averaged hygroscopicity (κ). The slope of the CCN efficiency spectra was found to be steep and similar to that for pure $(NH_4)_2SO_4$ particles, indicating homogeneity in the mixing states of the aerosol particles. Particles much larger than 100 nm were found to be activated at all investigated values of SS regardless of their composition, whereas particles < 40 nm required out-of-range (higher) SS for activation. Activation diameter for both the particles were found to be decreasing with increase in SS. Due to homogeneity of aerosols, the hygroscopicity parameter does not show any specific trend with SS or activation diameter. Experimentally measured activation diameter at examined SS levels for both these salts were found to be in good agreement with the theoretical estimations. However, comparison of size-averaged hygroscopicity showed slight variation at higher SS levels. Although well documented for the particles of environmental significance, this kind of study has been performed for the first time for the particles which are relevant to nuclear reactor accident analysis. As the reactor environment may have supersaturating conditions during and after a postulated reactor accidents, activation of released/converted fission product particles i.e., CsI and CsOH can not be ruled out. Accuracy of the deposition rates in reactor component systems and environmental source term estimations in postulated accident scenarios will get improved, if CCN properties of CsI and CsOH particles are taken into account. These results supplement the database of characteristics of particles of nuclear reactor relevance and should be assisting the simulations made by nuclear safety codes such as ASTEC, MELCOR or RELAP6.

Declaration of Competing Interest

None.

Acknowledgement

The authors gratefully acknowledge the financial support from the Board of Research in Nuclear Science (BRNS), Department of Atomic Energy (DAE), Government of India to conduct this research under project no. 36(2,4)/15/01/2015-BRNS. The authors are also thankful to Mr. Akarsh Ralhan, IISER Bhopal, India, for helping us in the experiments.

References

Acquista, N., Abramowitz, S., Lide, D.R., 1968. Structure of the alkali hydroxides. ii. the infrared spectra of matrixisolated csoh and csod. J. Chem. Phys. 49 (2), 780–782.
Allelein, H.J., Auvinen, A., Ball, J., 2009. State-of-the-art report on nuclear aerosols. In: (NEA/CSNI/R(2009)5) NUCLEAR ENERGY AGENCY.
Andreae, M.O., Rosenfeld, D., Artaxo, P., Costa, A.A., Frank, G.P., Longo, K.M., Silva-Dias, M.A.F., 2004. Smoking rain clouds over the amazon. Science 303 (5662), 1337–1342.
Andreae, M.O., Jones, C.D., Cox, P.M., 2005. Strong present-day aerosol cooling implies a hot future. Nature 435, 1187–1190.
Andreae, M.O., Hegg, D., Feichter, J., Kloster, S., Levin, Z., Li-ousse, C., Radke, L., Stier, P., 2007. Sources and nature of atmospheric aerosols. In: Levin, Z., Cotton, W. (Eds.), Scientific assessment of the effects of aerosols on precipitation. World Meteorological Organization.
Badawi, M., Xerri, B., Canneaux, S., Cantrel, L., Louis, F., 2012. Molecular structures and thermodynamic properties of 12 gaseous cesium-containing species of nuclear safety interest: Cs2, csh, cso, cs2o, csx, and cs2x2 (x = oh, cl, br, and i). J. Nucl. Mater. 420 (1), 452–462.
Bhattu, D., Tripathi, S.N., 2014. Inter-seasonal variability in size-resolved ccn properties at Kanpur, India. Atmos. Environ. 85, 161–168.
Bhattu, D., Tripathi, S.N., 2015. Ccn closure study: effects of aerosol chemical composition and mixing state. J. Geophys. Res. Atmos. 120, 766–783.
Bhattu, D., Tripathi, S., Chakraborty, A., 2016. Deriving aerosol hygroscopic mixing state from size-resolved ccn activity and hr-tof-ams measurements. Atmos. Environ. 142, 57–70.
Camata, R.P., Hirasawa, M., Okuyama, K., Takeuchi, K., 2000. Observation of aerosol formation during laser ablation using a low-pressure differential mobility analyzer. J. Aerosol Sci. 31 (4), 391–401.
Charlson, R.J., Seinfeld, J.H., Nenes, A., Kulmala, M., Laaksonen, A., Facchini, M.C., 2001. Reshaping the theory of cloud formation. Science 292, 2025–2026.
Che, H., Zhang, X., Zhang, L., Wang, Y., Zhang, Y., Shen, X., Ma, Q., Sun, J., Zhong, J., 2017. Prediction of size-resolved number concentration of cloud condensation nuclei and long-term measurements of their activation characteristics. Sci. Rep. 7 (1), 5819.
Dalirian, M., Keskinen, H., Ahlm, L., Ylisirniö, A., Romakkaniemi, S., Laaksonen, A., Virtanen, A., Riipinen, I., 2015. Ccn activation of fumed silica aerosols mixed with soluble pollutants. Atmos. Chem. Phys. 15 (7), 3815–3829.
Davidson, C.I., Stephenson, M., Monaghan, M., Pudykiewicz, J., Schell, W., et al., 1987. Radioactive cesium from the Chernobyl accident in the Greenland ice sheet. Science 237 (4815), 633–634.
Duan, J., Wang, Y., Xie, X., Li, M., Tao, J., Wu, Y., Cheng, T., Zhang, R., Liu, Y., Li, X., He, Q., Gao, W., Wang, J., 2018. Influence of pollutants on activity of aerosol cloud condensation nuclei (ccn) during pollution and post-rain periods in Guangzhou, southern China. Sci. Total Environ. 642, 1008–1019.
Dwivedi, A., Khan, A., Tripathi, S., Joshi, M., Mishra, G., Nath, D., Tiwari, N., Sapra, B., 2019. Aerosol depositional characteristics in piping assembly under varying flow conditions. Prog. Nucl. Energy 116, 148–157.
Frank, G.P., Dusek, U., Andreae, M.O., 2006. Technical note: a method for measuring size-resolved ccn in the atmosphere. Atmos. Chem. Phys Discuss. 6, 4879–4895.
Garland, J., 1969. Condensation on ammonium sulphate particles and its effect on visibility. Atmos. Environ. 3 (3), 347–354.
Gunthe, S.S., King, S.M., Rose, D., Chen, Q., Roldin, P., Farmer, D.K., Jimenez, J.L., Artaxo, P., Andreae, M.O., Martin, S.T., Pöschl, U., 2009. Cloud condensation nuclei in pristine tropical rainforest air of Amazonia: size-resolved measurements and modeling of atmospheric aerosol composition and ccn activity. Atmos. Chem. Phys. 9 (19), 7551–7575.
Hiranuma, N., Kohn, M., Pekour, M.S., Nelson, D.A., Shilling, J.E., Cziczo, D.J., 2011. Droplet activation, separation, and compositional analysis: laboratory studies and atmospheric measurements. Atmos. Meas. Tech. 4 (10), 2333–2343.
Hudson, J.G., Noble, S., 2014a. Ccn and vertical velocity influences on droplet concentrations and supersaturations in clean and polluted stratus clouds. J. Atmos. Sci. 71 (1), 312–331.
Hudson, J.G., Noble, S., 2014b. Low-altitude summer/winter microphysics, dynamics, and ccn spectra of northeastern caribbean small cumuli, and comparisons with stratus. J. Geophys. Res. Atmos. 119 (9), 5445–5463.
Hudson, J.G., Xie, Y., 1999. Vertical distributions of cloud condensation nuclei spectra over the summertime northeast pacific and Atlantic oceans. J. Geophys. Res. Atmos. 104 (D23), 30219–30229.
Hudson, J.G., Yum, S.S., 2002. Cloud condensation nuclei spectra and polluted and clean clouds over the indian ocean. J. Geophys. Res. Atmos. 107 (D19), INX2–21.
Inade, Y., Akagane, K., 1996. Non-empirical study of chemical reactions including fission products in severe light water reactor accidents. J. Nucl. Sci. Technol. 33 (7), 562–568.
Izrael, Y.A., Cort, M.D., Jones, A., Nazarov, I., Fridman, S.D., Kvasnikova, E., Stukin, E., Kelly, G., Matveenko, I., Pokumeiko, Y.M., et al., 1996. The Atlas of Cesium-137 Contamination of Europe after the Chernobyl Accident.
Jokiniemi, J., 1988. The growth of hygroscopic particles during severe core melt accidents. Nucl. Technol. 83 (1), 16–23.
Jokiniemi, J., 1990. Effect of selected binary and mixed solutions on steam condensation and aerosol behavior in containment. Aerosol Sci. Technol. 12 (4), 891–902.
Koehler, K.A., DeMott, P.J., Kreidenweis, S.M., Popovicheva, O.B., Petters, M.D., Carrico, C.M., Kireeva, E.D., Khokhlova, T.D., Shonija, N.K., 2009. Cloud condensation nuclei and ice nucleation activity of hydrophobic and hydrophilic soot particles. Phys. Chem. Chem. Phys. 11, 7906–7920.
Koulikov, A., Ryabov, I., 1992. Specific cesium activity in freshwater fish and the size effect. Sci. Total Environ. 112 (1), 125–142.
Kreidenweis, S.M., Koehler, K., DeMott, P.J., Prenni, A.J., Carrico, C., Ervens, B., 2005. Water activity and activation diameters from hygroscopicity data - part i: Theory and application to inorganic salts. Atmos. Chem. Phys. 5 (5), 1357–1370.
Kuczkowski, R.L., Lide Jr., D.R., Krisher, L.C., 1966. Microwave spectra of alkali hydroxides: Evidence for linearity of csoh and koh. J. Chem. Phys. 44 (8), 3131–3132.
Lathem, T.L., Nenes, A., 2011. Water vapor depletion in the dmt continuous-flow ccn chamber: effects on supersaturation and droplet growth. Aerosol Sci. Technol. 45 (5), 604–615.
Lavi, N., Golob, G., Alfassi, Z., 2006. Monitoring and surveillance of radio-cesium in cultivated soils and foodstuff samples in Israel 18 years after the Chernobyl disaster. Radiat. Meas. 41 (1), 78–83.
Li, R.-Z., Liu, C.-W., Gao, Y.Q., Jiang, H., Xu, H.-G., Zheng, W.-J., 2013. Microsolvation of lii and csi in water: anion photoelectron spectroscopy and ab initio calculations. J. Am. Chem. Soc. 135 (13), 5190–5199 PMID: 23432353.
Li, Y., Tasoglou, A., Liangou, A., Cain, K.P., Jahn, L., Gu, P., Kostenidou, E., Pandis, S.N., 2018. Cloud condensation nuclei activity and hygroscopicity of fresh and aged cooking organic aerosol. Atmos. Environ. 176, 103–109.

Loftus, A., Cotton, W., 2014. Examination of ccn impacts on hail in a simulated supercell storm with triple-moment hail bulk microphysics. Atmos. Res. 147–148, 183–204.
Long, N., Truong, Y., Hien, P., Binh, N., Sieu, L., Giap, T., Phan, N., 2012. Atmospheric radionuclides from the fukushima dai-ichi nuclear reactor accident observed in vietnam. J. Environ. Radioact. 111, 53–58 (Environmental Impacts of the Fukushima Accident (Part I)).
Madoz-Escande, C., Garcia-Sanchez, L., Bonhomme, T., Morello, M., 2005. Influence of rainfall characteristics on elimination of aerosols of cesium, strontium, barium and tellurium deposited on grassland. J. Environ. Radioact. 84 (1), 1–20.
Mattsson, S., Moberg, L., 1991. Fallout from Chernobyl and atmospheric nuclear weapons tests. Chernobyl in perspective. In: Moberg, L. (Ed.), The Chernobyl Fallout in Sweden-Results from a Research Programme on Environmental Radiology. Swedish Radiation Protection Institute, Stockholm, pp. 591–627.
McFarlane, J., Wren, J.C., Lemire, R.J., 2002. Chemical speciation of iodine source term to containment. Nucl. Technol. 138 (2), 162–178.
McFiggans, G., Artaxo, P., Baltensperger, U., Coe, H., Facchini, M.C., Feingold, G., Fuzzi, S., Gysel, M., Laaksonen, A., Lohmann, U., Mentel, T.F., Murphy, D.M., O'Dowd, C.D., Snider, J.R., Weingartner, E., 2006. The effect of physical and chemical aerosol properties on warm cloud droplet activation. Atmos. Chem. Phys. 6 (9), 2593–2649.
Mishra, G., Mandariya, A.K., Tripathi, S., Mariam, Joshi, M., Khan, A., Sapra, B., 2019. Hygroscopic growth of csi and csoh particles in context of nuclear reactor accident research. J. Aerosol Sci. 132, 60–69.
Paasikallio, A., Rantavaara, A., Sippola, J., 1994. The transfer of cesium-137 and strontium-90 from soil to food crops after the Chernobyl accident. Sci. Total Environ. 155 (2), 109–124.
Padró, L.T., Moore, R.H., Zhang, X., Rastogi, N., Weber, R.J., Nenes, A., 2012. Mixing state and compositional effects on ccn activity and droplet growth kinetics of size-resolved ccn in an urban environment. Atmos. Chem. Phys. 12 (21), 10239–10255.
Petters, M.D., Kreidenweis, S.M., 2007. A single parameter representation of hygroscopic growth and cloud condensation nucleus activity. Atmos. Chem. Phys. 7 (8), 1961–1971.
Petti, D.A., 1989. Silver-indium-cadmium control rod behavior in severe reactor accidents. Nucl. Technol. 84 (2), 128–151.
Pringle, K.J., Tost, H., Pozzer, A., Pöschl, U., Lelieveld, J., 2010. Global distribution of the effective aerosol hygroscopicity parameter for ccn activation. Atmos. Chem. Phys. 10 (12), 5241–5255.
Ramana, M., 2006. Twenty years after Chernobyl: debates and lessons. Econ. Polit. Wkly. 1743–1747.
Ran, L., Deng, Z., Ju, J., Sun, H., Liu, J., Lin, W., Tian, P., Liu, Q., Huang, M., Wang, P., Xia, X., Pan, W., Gao, W., Xu, W., Xu, X., 2019. Femtosecond filamentation induced particles and their cloud condensation nuclei activity. Atmos. Environ. 206, 271–279.
Rose, D., Gunthe, S.S., Mikhailov, E., Frank, G.P., Dusek, U., Andreae, M.O., Pöschl, U., 2008. Calibration and measurement uncertainties of a continuous-flow cloud condensation nuclei counter (dmt-ccnc): Ccn activation of ammonium sulfate and sodium chloride aerosol particles in theory and experiment. Atmos. Chem. Phys. 8 (5), 1153–1179.
Rose, D., Nowak, A., Achtert, P., Wiedensohler, A., Hu, M., Shao, M., Zhang, Y., Andreae, M.O., Pöschl, U., 2010. Cloud condensation nuclei in polluted air and biomass burning smoke near the mega-city Guangzhou, China part 1: Size-resolved measurements and implications for the modeling of aerosol particle hygroscopicity and ccn activity. Atmos. Chem. Phys. 10 (7), 3365–3383.
Rosenfeld, D., Givati, A., 2006. Evidence of orographic precipitation suppression by air pollutioninduced aerosols in the western United States. J. Appl. Meteorol. Climatol. 45 (7), 893–911.
Segal, Y., Khain, A., Nenes, A., Pinsky, M., Sterkin, A., 2004. Sensitivity of rain-drop formation in ascending cloud parcels to cloud condensation nuclei and thermodynamic conditions. Q. J. Roy. Meteorol. Soc. 130, 561–581.
Stohl, A., Seibert, P., Wotawa, G., Arnold, D., Burkhart, J.F., Eckhardt, S., Tapia, C., Vargas, A., Yasunari, T.J., 2012. Xenon-133 and caesium-137 releases into the atmosphere from the Fukushima dai-ichi nuclear power plant: determination of the source term, atmospheric dispersion, and deposition. Atmos. Chem. Phys. 12, 2313–2343.
Tang, M., Guo, L., Bai, Y., Huang, R.-J., Wu, Z., Wang, Z., Zhang, G., Ding, X., Hu, M., Wang, X., 2019. Impacts of methanesulfonate on the cloud condensation nucleation activity of sea salt aerosol. Atmos. Environ. 201, 13–17.
Thomas, A., Martin, J., 1986. First assessment of Chernobyl radioactive plumes over Paris. Nature (London) 321 (6073), 817–819.
Twohy, C.H., Hudson, J.G., Yum, S.-S., Anderson, J.R., Durlak, S.K., Baumgardner, D., 2001. Characteristics of cloud-nucleating aerosols in the indian ocean region. J. Geophys. Res. Atmos. 106 (D22), 28699–28710.
Vakulovsky, S., Nikitin, A., Chumichev, V., Katrich, I.Y., Voitsekhovich, O., Medinets, V., Pisarev, V., Bovkum, L., Khersonsky, E., 1994. Cesium-137 and strontium-90 contamination of water bodies in the areas affected by releases from the Chernobyl nuclear power plant accident: an overview. J. Environ. Radioact. 23 (2), 103–122.
Wright, A., 1994. Primary system fission product release and transport: a state-of-the-art report to the committee on the safety of nuclear installations. In: NUREG/CR–6193.
Yoschenko, V., Kashparov, V., Levchuk, S., Glukhovskiy, A., Khomutinin, Y., Protsak, V., Lundin, S., Tschiersch, J., 2006. Resuspension and redistribution of radionuclides during grassland and forest fires in the Chernobyl exclusion zone: part ii. modeling the transport process. J. Environ. Radioact. 87 (3), 260–278.
Yum, S.S., Hudson, J.G., 2001. Vertical distributions of cloud condensation nuclei spectra over the springtime arctic ocean. J. Geophys. Res. Atmos. 106 (D14), 15045–15052.
Yum, S.S., Hudson, J.G., 2004. Wintertime/summertime contrasts of cloud condensation nuclei and cloud microphysics over the southern ocean. J. Geophys. Res. Atmos. 109 (D6).